REX and RECOMMANDATIONS FOR MECHANICAL INTEGRATION OF LARGE HIGH-SPEED MOTORS

Paper No. PCIC Europe EUR23_24

Lionel Durantay, PhD
Senior Member, IEEE
GE Power Conversion
442, rue de la Rompure
54250 Champigneulles
France
lionel.durantay@ge.com

Alain Gelin, PhD
Member, IFToMM
TotalEnergies
Avenue Larribau
64018 Pau
France
alain.gelin@totalenergies.com

Edouard Thibaut
Member, IEEE
TotalEnergies
2, place Jean Millier
92078 Paris
France
edouard.thibaut@totalenergies.com

Lionel Roth
GE Power Conversion
442, Rue de la Rompure
54250 Champigneulles
France
lionel.roth@ge.com

Abstract – Synchronous and asynchronous motor technologies dedicated to high speed make it possible to offer high-power variable-speed compression services without using gearboxes. The mechanical integration of these motors requires special precautions because of the wide speed variation ranges required. The first part of this paper explains the mechanical integration rules described in the API 541 and 546 standards which are the most restrictive in the world, and rotating machines signatures of vibrations in case of mechanical looseness. The main linear and non-linear dynamic mechanisms related to electrical machines are also explained. The second part describes a site return of experience from a vibratory instability of an 15MW 2-pole motor and explains the mechanism that led to this instability. The third part proposes the recommendations to be followed for synchronous or induction motor by manufacturer, OEM, EPC and User-End in terms of modelling, design and testing for successful mechanical integration and is illustrated by a two business cases of high-speed induction motor fed by Voltage Source Inverter.

Index – Synchronous Motor, Induction Motor, Rotordynamics, Non-linear resonance, Instability.

I. INTRODUCTION

The standalone direct drive systems are now used for most of services of compression, including starter-helper compression trains (Fig.1) and are also an alternative to gas or steam turbines mechanical drivers with full electric compression.

Fig.1. 20MW induction motor integrated on LNG Train [1].

The architecture is based on 2-pole wound synchronous or induction squirrel cage motor on oil lubricated bearings fed by VSD, directly driven the compressors without intermediate gearbox (Fig.2). Whatever the polarity of motors, the API 541 5th edition for asynchronous motors and API546 4th edition for synchronous motors require the same separation margins to avoid the risk of vibrations by resonance mechanisms. The API requires that the frame of the completely assembled machine on its permanent foundation with the rotor installed and rotating shall be free from structural resonance between 40% and 60% of operating speed (Ω_{op}) and the exclusion speed ranges defined by the following equations:

$$\langle \Omega_{op} \rangle = n.\Omega_{op} \pm 0.15\ \Omega_{op} \quad \text{where } n = 1 \text{ and } 2 \qquad (1)$$

$$\langle \Omega_{el} \rangle = n.\Omega_{el} \pm 0.15\ \Omega_{el} \quad \text{where } n = 1 \text{ and } 2 \qquad (2)$$

Ω_{op} for variable speed machine is the speed range piloted by the drive, usually 70% to 105% of the rated speed.

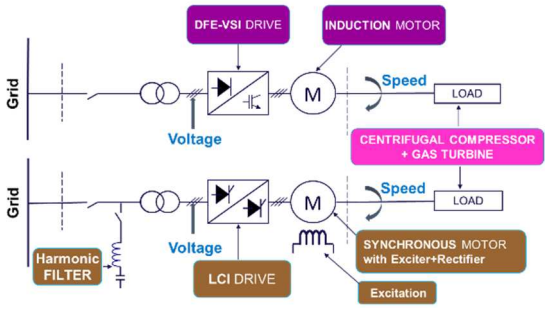

Fig.2. Examples of electric direct drive architectures.

Massive foundation is recommended by the API. The rigidity of a foundation is a relative quantity. It should be compared with the rigidity of the machine bearing system. The ratio of housing vibration to foundation vibration is a characteristic quantity for the evaluation of foundation flexibility influences. One indication that a foundation is massive if the vibration amplitudes of the foundation near the machine feet or base frame are less than 30% of the amplitudes that could be measured at the adjacent bearing housing.

The specialized machinery vibration analysis literature [2] describes the main defects of rotating machinery vibrations such as unbalance, misalignment, resonance, mechanical looseness. Mechanical looseness can occur at the three locations:

- Internal assembly looseness for instance due to clearance between bearing housing and sleeves,
- Structure looseness because of cracks,
- Looseness at machine to base plate interface for instance due to the rocking motion of the pillow block with loose bolts, weakness in the machine feet, baseplate, or foundation.

It caused to an improper fit between components, producing many harmonics in the FFT due to non-linear

response of the loose parts to the exciting forces from the rotor. The vibrations are often unstable and can vary in a chaotic way from one measurement to the next. Looseness will often cause sub-harmonics multiples at 0.5X, 1.5X, 2.5X in addition to 1X, 2X, 3X harmonics. The mechanisms for generating these sub-synchronous frequencies are generally not explained in these maintenance tables. This will be the subject of the next chapter.

II. NON-LINEAR VIBRATORY MODELS FOR ELECTRIC MOTORS

A. Second Order Linear Dynamic Model

In physics, the fundamental equation of the dynamics which links the force (cause) to the displacement (response), is modeled by an equivalent system of the second order where (M), (D) and (K) are respectively the terms of inertia, damping and stiffness (Fig.3). In the case of a linear model, these terms are considered constant.

$$\mathrm{M}.\ddot{\mathrm{U}}(\mathrm{t}) + \mathrm{D}.\dot{\mathrm{U}}(\mathrm{t}) + \mathrm{K}.\mathrm{U}(\mathrm{t}) = \mathrm{F}(\mathrm{t}) \quad (3)$$

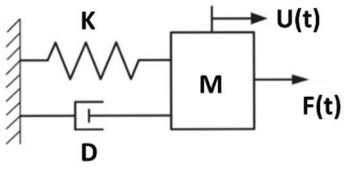

Fig.3. Equivalent second order mechanical system.

In the case of a rotordynamics model, the equivalent term of stiffness is the serialization of the stiffness of the rotor with those of the bearings:

$$\mathrm{K} = (\mathrm{K}_{\mathrm{Rotor}}^{-1} + \mathrm{K}_{\mathrm{Bearings}}^{-1})^{-1} \quad (4)$$

The characteristic equation has complex roots $(\bar{\lambda})$ whose real part (λ_{Re}) is the damping term, and imaginary part (λ_{Im}) is the damped natural pulsation:

$$\mathrm{M}.\bar{\lambda}^2 + \mathrm{D}.\bar{\lambda} + \mathrm{K} = 0 \quad (5)$$

$$\text{where} \quad \bar{\lambda} = \lambda_{\mathrm{Re}} \pm \mathrm{j}.\lambda_{\mathrm{Im}} = \frac{-\mathrm{D}}{2.\mathrm{M}} \pm \mathrm{j}\sqrt{\frac{\mathrm{K}}{\mathrm{M}} - \frac{\mathrm{D}^2}{4.\mathrm{M}^2}} \quad (6)$$

The reduced form of the equation in which (ζ) is the critical damping fraction and (ω_0) the critical undamped critical (or natural) pulsation is given as follows:

$$\ddot{\mathrm{U}}(\mathrm{t}) + 2.\zeta.\omega_0\,\dot{\mathrm{U}}(\mathrm{t}) + {\omega_0}^2.\mathrm{U}(\mathrm{t}) = \mathrm{F}(\mathrm{t})/\mathrm{M} \quad (7)$$

$$\text{where} \quad \zeta = \frac{\mathrm{D}}{2.\sqrt{\mathrm{K}.\mathrm{M}}} \quad \text{and} \quad \omega_0 = \sqrt{\frac{\mathrm{K}}{\mathrm{M}}} \quad (8)$$

The solution $\mathrm{U}(\mathrm{t})$ of the equation finally has the following form where (U_0) and (φ) are constants of integration:

$$\mathrm{U}(\mathrm{t}) = \mathrm{U}_0.\exp\left(\frac{(-\mathrm{D})}{2.\mathrm{M}}\mathrm{t}\right).\sin\left\{\left(\omega_0.\sqrt{1 - \frac{(-\mathrm{D})^2}{4.\mathrm{K}}}.\mathrm{t}\right) + \varphi\right\} \quad (9)$$

As $(\zeta<1)$ then the system is hyper-damped or pseudo-periodic. In other words, the system is stable with a displacement $\mathrm{U}(\mathrm{t})$ amplified at resonance by an amplification factor equal to:

$$\mathrm{AF}=1/(2.\zeta) \quad (10)$$

B. Second Order Non-Linear Dynamic Model

If the coefficients of the differential equation are not constant but depend on time, then the equation becomes non-linear [3]:

$$\mathrm{M}(\mathrm{t}).\ddot{\mathrm{U}}(\mathrm{t}) + \mathrm{D}(\mathrm{t}).\dot{\mathrm{U}}(\mathrm{t}) + \mathrm{K}(\mathrm{t}).\mathrm{U}(\mathrm{t}) = \mathrm{F}(\mathrm{t}) \quad (11)$$

The reduced form of the equation is of the following form where the time dependence function f(t) can be factored:

$$\ddot{\mathrm{U}}(\mathrm{t}) + 2.\zeta.\omega_0\,\dot{\mathrm{U}}(\mathrm{t}) + {\omega_0}^2.\mathrm{f}(\mathrm{t}).\mathrm{U}(\mathrm{t}) = \mathrm{F}(\mathrm{t})/\mathrm{M} \quad (12)$$

This equation was introduced by George William Hill in 1886 and comes up recurrently in physics. One can always, using a change of variable, obtain a similar equation where f(t) is periodic, rewrites it as a Fourier serie:

$$\mathrm{f}(\mathrm{t}) = \mathrm{a}_0 + \sum_{\mathrm{n}} \mathrm{a}_{\mathrm{n}}.\cos(\mathrm{n}\Omega\mathrm{t} + \Phi_{\mathrm{n}}) \quad (13)$$

Émile Léonard Mathieu, French mathematician living in Nancy, worked on the properties of this equation. Depending on the exact shape of f(t), solutions may stay bounded for all time, or the amplitude of the oscillations in solutions may grow exponentially. The equation induces a set of instability bands $\langle \mathrm{I}_{\mathrm{n}} \rangle$ centered on non-integer ranks of the eigenvalue $(\bar{\lambda})$:

$$\langle \mathrm{I}_{\mathrm{n}} \rangle = \frac{\mathrm{n}}{2}.\bar{\lambda} \pm \Delta_{\mathrm{n}}(\omega_0, \zeta, \mathrm{a}_{\mathrm{n}}, \Phi_{\mathrm{n}}) \quad (14)$$

The 1X and 2X excitation forces of the rotor, combined to the pole passing frequency excitation at twice motor frequency ($2xf_s$) can produce a broad spectrum of dynamic response with sub-harmonics and harmonics that are unstable, even chaotic.

C. Example of Non-Linear Rotor

An example of a rotor inducing periodic coefficients in the dynamic's equation is a synchronous 2-pole rotor. The cross-section of the rotor shows two main directions in the axis of the poles (η) and in the axis of the slots of coils (ξ) [4]. This rotor is anisotropic (Fig.4 & 5). The coefficients are constant for a squirrel-cage induction rotor because the rotor cross-section is symmetrical in both directions (η) and (ξ). The squirrel cage rotor is isotropic (Fig.5):

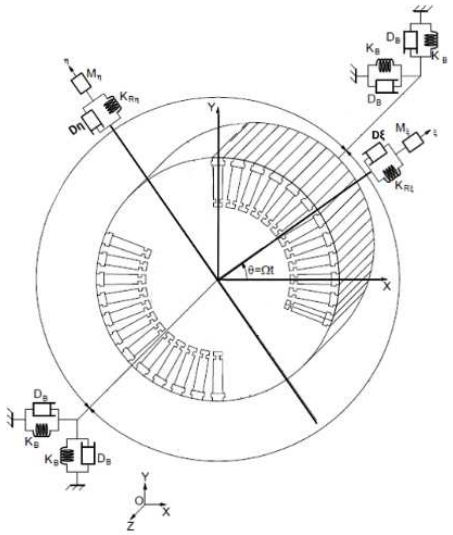

Fig.4. 2-pole turbo synchronous rotor model.

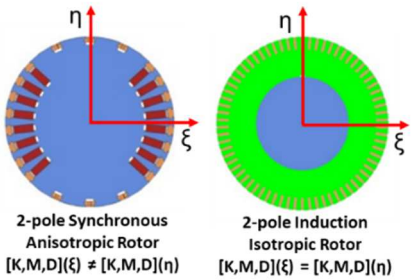

Fig.5. 2-pole synchronous vs 2-pole induction cross sections of rotor.

The mass $M(t)$ and stiffness $K(t)$ of the 2-pole synchronous rotor is modeled by a π-periodic function with the following formulas where (Ω) is the rotational pulsation:

$$M(t) = \left(\frac{M_\xi + M_\eta}{2}\right) + \left\{\left(\frac{|M_\xi - M_\eta|}{2}\right).\cos(2.\Omega.t)\right\} \quad (15)$$

$$K(t) = \left(\frac{K_\xi + K_\eta}{2}\right) + \left\{\left(\frac{|K_\xi - K_\eta|}{2}\right).\sin(2.\Omega.t)\ \right\} \quad (16)$$

We can define from the characteristic polynomial of this Mathieu's equation a term of circular pulsation (ω_{a0}) and a term of asymmetry (μ) from the two critical pulsations of anisotropy (ω_ξ) and (ω_η):

$$\omega_{a0}^2 = \frac{\omega_\xi^2 + \omega_\eta^2}{2} \text{ where } \omega_\xi = \sqrt{\frac{K_\xi}{M_\xi}} \text{ and } \omega_\eta = \sqrt{\frac{K_\eta}{M_\eta}} \quad (17)$$

$$\mu = \frac{|\omega_\xi^2 - \omega_\eta^2|}{2.\omega_0^2} \quad (18)$$

A term homogeneous with an internal damping (D_I) of the rotor is defined by passing from the rotating axis (ξ,η) to the fixed axis (X,Y), according to the anisotropic dampings (D_ξ) and (D_η):

$$D_I = \left|\sqrt{K_\xi.M_\xi} - \sqrt{K_\eta.M_\eta}\right| = \left|D_\xi - D_\eta\right| \quad (19)$$

The differential equation in the fixed axis is the following where (D_I) subtracts from (D):

$$M.\ddot{U}(t) + (D - D_I).\dot{U}(t) + K.U(t) = F(t) \quad (20)$$

The solution $U(t)$ of the equation has the following form:

$$U(t) = U_0.\exp\left(\frac{(D_I - D)}{2.M}t\right).\sin\left\{\left(\omega_{a0}.\sqrt{1 - \frac{(D_I - D)^2}{4.K}}.t\right) + \varphi\right\} \quad (21)$$

The displacement is stable only if $(D - D_I) > 0$ (22)

The equation induces a set of instability bands $\langle I_n \rangle$ centered on non-integer ranks of the circular pulsation (ω_{a0}). The more the rotor is asymmetrical with deep winding notches, the more the system will be sensitive to sub-synchronous and synchronous parametric excitations, see instabilities if there are interactions with close natural frequencies:

$$\langle I_n \rangle = \left[\frac{n}{2}\omega_{a0}.\sqrt{1-\mu}\ ,\frac{n}{2}\omega_{a0}.\sqrt{1+\mu}\right] \quad (23)$$

In general, an electrical rotor or a mechanical rotor such as a compressor, becomes unstable if in certain conditions the internal damping of the rotor is greater in absolute value than the damping of the fixed parts of the system, mainly provided by the oil film of the bearings.

D. Conditions of stability and instability of a rotor

By generalization, the differential equation linking the force to the displacement can be split into an inertia effect $(\overrightarrow{F_M})$, a stiffness effect $(\overrightarrow{F_K})$, a damping effect $(\overrightarrow{F_D})$, an instability effect $(\overrightarrow{F_{D_I}})$:

$$\overrightarrow{F(t)} = \overrightarrow{F_0}.e^{-j\Omega t} = \left(\overrightarrow{F_M} + \overrightarrow{F_D} + \overrightarrow{F_{D_I}} + \overrightarrow{F_K}\right).e^{-j\Omega t} \quad (24)$$

$$\text{where } \overrightarrow{F_K} = K.\overrightarrow{U_0} \text{ and } \overrightarrow{F_M} = M.\Omega^2.e^{+j\pi}.\overrightarrow{U_0} \quad (25)$$

$$\overrightarrow{F_D} = D.\Omega.e^{-j\frac{\pi}{2}}.\overrightarrow{U_0} \text{ and } \overrightarrow{F_{D_I}} = D_I.\Omega.e^{+j\frac{\pi}{2}}.\overrightarrow{U_0} \quad (26)$$

As if driving a car, the damping and instability forces, parallel to the trajectory, have the action of a brake and accelerator pedal respectively (Fig.6).

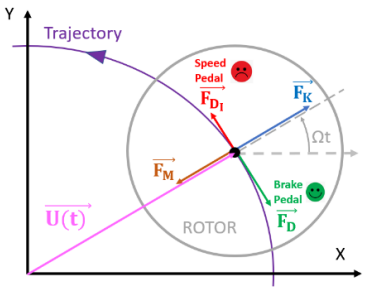

Fig.6. Vectorial system of forces applied to the rotor.

By introducing the Complex Dynamic Stiffness (CDS) between the excitation force and the displacement response, it is possible to represent the four different response cases of the system depending on the excitation frequency (Ω) [5, 6]:

$$\overrightarrow{F(t)} = CDS(\Omega).\overrightarrow{U(t)} \quad (27)$$

$$\text{where } CDS(\Omega) = (K - M.\Omega^2) + j.(D - D_I).\Omega \quad (28)$$

- **Case #A** ➔ At low excitation frequency ($\Omega \ll \omega_0$), the dominant component of the CDS is the static stiffness (K). The response amplitude $\overrightarrow{U(t)}$ practically do not differ from the static force $\overrightarrow{F(t)}$. The system is stable (Fig.7).

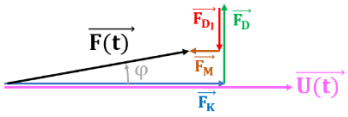

$\vec{F}$ // $\vec{U}$ driven by System Stiffness
➔ **STABLE DISPLACEMENT**

Fig.7. Low excitation frequency - Fresnel diagram

- **Case #B** ➔ At high excitation frequency ($\Omega \gg \omega_0$), the most significant term in the CDS is the inertia term (M). The response $\overrightarrow{U(t)}$ differs by almost 180° from the force $\overrightarrow{F(t)}$. The system is stable (Fig.8).

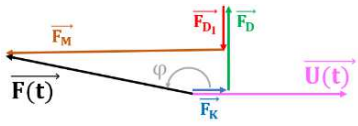

$\vec{F}$ // $\vec{U}$ driven by System Inertia
➔ **STABLE DISPLACEMENT**

Fig.8. High excitation frequency - Fresnel diagram.

- **Case #C** ➔ At frequency excitation close to the system resonance $(\Omega \approx \omega_0)$, the real part of the CDS is close to zero. The response $\overrightarrow{U(t)}$ is perpendicular, in direct quadrature +90° with respect to the force. The amplitude of the response is limited by the damping (D) of the mode. If the rotor produces internal rotor damping, (D_I) then the system response is further amplified. The system is resonant but remains stable (Fig.9).

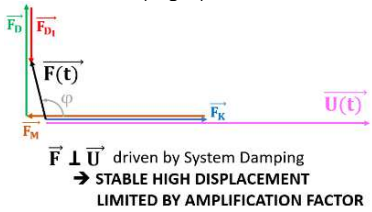

Fig.9. Resonance frequency Fresnel diagram with low rotor internal damping.

- **Case #D** ➔ If the internal damping of the rotor $(\overrightarrow{F_{D_I}})$ (accelerator pedal) becomes greater than the external damping $(\overrightarrow{F_D})$ (brake pedal), close to the system resonance $(\Omega \approx \omega_0)$,, then the trajectory will amplify and become unstable. The response is in inverse quadrature -90° with the excitation force. The system is resonant, unstable and can become chaotic (Fig.10).

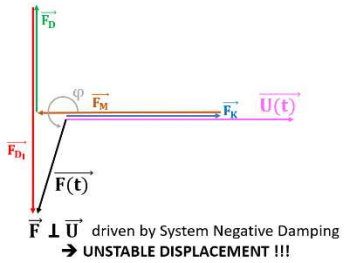

Fig.10. Resonance frequency Fresnel diagram with high rotor internal damping.

III. THREE RETURNS OF EXPERIENCE

A. Business Case #1

1. Factory Acceptance Tests

The first business case concerns the integration of a 15MW 2-pole induction motors operating in a variable speed range from 3420 rpm to 3626 rpm, used as a starter-helper of compression train for an LNG site in the United States. The bearings sleeves are 4-lobe oil-lubricated. The API is the standard for this project. For the FAT tests, the motors are mounted on rigid soleplates in accordance with the API 541 recommendation. The vibration tests are carried out at no load, and under load, with slowing down tests. The motors are accepted with low residual vibrations, thermal unbalance, shaft displacements in accordance with API 541 (Fig.11). In accordance with rotordynamics simulation, the two natural frequencies of rotor bending are around 30 Hz and 35 Hz. For a fixed speed motor, the API requires a band of frequency exclusion between 40% and 60% of rated speed. For a variable speed motor this constraint is impossible to satisfy because the shaft bending modes for this type of rotor on oil bearings are always in frequencies between 25 Hz and 35 Hz. The resonance amplitudes not exceeding 50 umpp, motors are accepted.

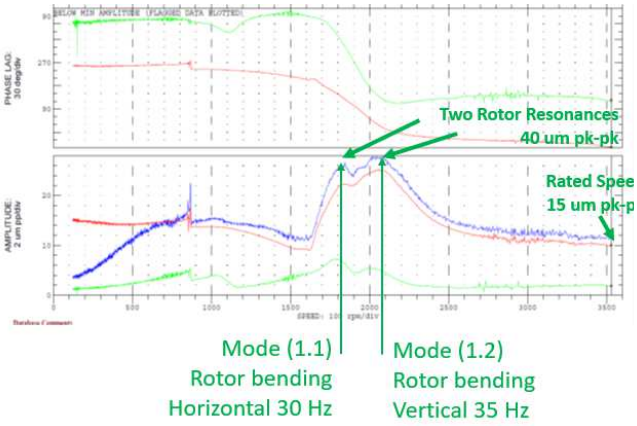

Fig.11. Rigid foundation – Speed Ramp-up (FAT).

2. Site Commissioning

On site, the machines are installed on their skids and foundations (Fig.12). During initial ramp-up trials, motor uncoupled, the vibrations at the bearings, motor feet and skid locations (Fig.13) are measured at 1000 rpm, 1750 rpm (speed close to critical speeds) and 3600 rpm (rated speed) (Table I). Whatever the speeds, the vibration ratio between the vibrations of the bearings and the feet of the motor are close to 1 and the vibrations between the top and the bottom of the skid are in the order of 0.2 to 0.1 that skids is the most flexible part of the system, considering API criteria. Vibrations passing bending modes are over 7 mm/s rms.

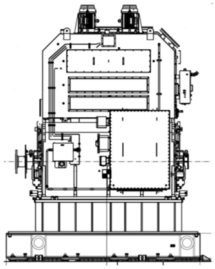

Fig.12. Skid + Motor.

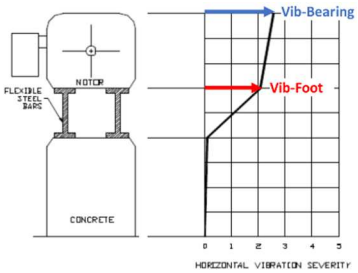

Fig.13. Example of flexible skid [8]

TABLE I
Horizontal Vibration Mapping

Speed (rpm)	1000	1750	3600
Motor Bearing Horizontal Vibration (mm/s rms)	1.4	7.1	3.8
Motor Foot Horizontal Vibration (mm/s rms)	1.3	7.0	3.7
Skid Horizontal Vibration (mm/s)	0.3	0.7	0.5
Foot / Bearing Vibration Ratio	0.92	0.98	0.97
Skid / Foot Vibration Ratio	0.23	0.10	0,13

Shaft Displacements when passing bending modes around 32 Hz are unstable and chaotic with amplitude above 200 umpp (Fig.14).

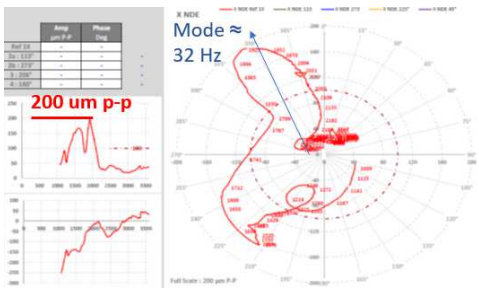

Fig.14. Nyquist vibrations during speed ramp-up (Site).

The bode diagram measured in speed ramp-up shows a frequency at 32Hz, between the 2 bending modes. (Fig.15) This frequency corresponds to the lateral reed mode of the system oscillating from portside to starboard (Fig.16).

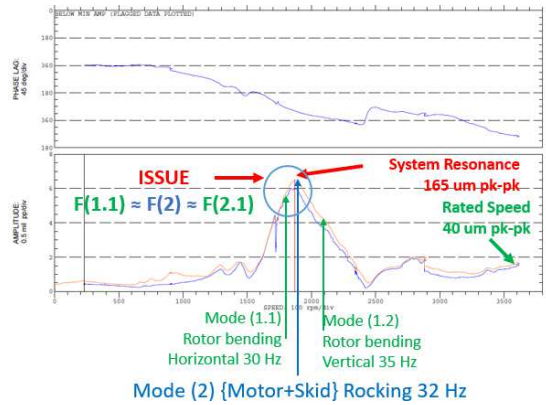

Fig.15. Flexible foundation – Speed Ramp-up (Site).

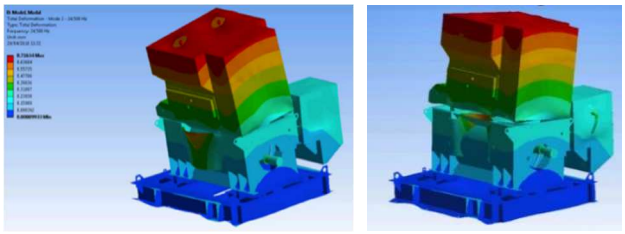

Fig.16. Example of system motion of reed mode [7].

The vibration measurements of shaft movements in transient speed regime and at stabilized speed @ 3600 rpm clearly show the activation of 0.5X and 1.5X sub-harmonics in addition to the 1X, 2X and 3X harmonics whose amplitudes continue to increase with constant phases, with global amplitude of the order of 140 umpp. A splitting of the natural resonances in 1X and 2X is also measured showing the evidence of parametric mechanisms (Fig.17):

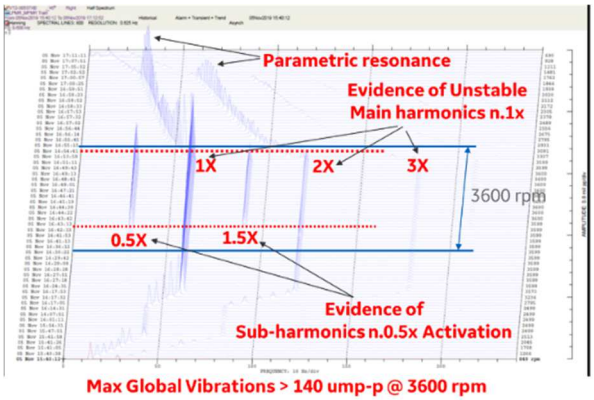

Fig.17. Shaft displacement waterfall.

The stability of the vibrations is recovered by stiffening as much as possible all the interfaces of shimming and bolting, knowing that all the attempts of balancing failed. This kind of instability linked to a reed mode interacting with the 1/2X sub-harmonic rank is described experimentally and practically in the literature, without theoretical demonstration [8]. Here is the scientific explanation of the phenomenon in our case. Due to its natural flexibility, the skid has its natural frequency at 32Hz. This natural frequency is coupled with the two natural frequencies of rotor bending at 30Hz and 35Hz. If the (1X) residual unbalance of the rotor excites these natural frequencies, there are periodic variations of stiffnesses $K_{fixation}(t)$ induced in all the fastening interfaces with chaotic shaft displacements. When the rotor is operating around 60Hz at twice these natural frequencies, there is activation of the parametric instability bands (Eq.14) due to the periodic non-linearity of the fixation stiffnesses due to the reed resonance mechanism at 0.5X. This frequency coupling amplifies the dynamic movements of structures and induces a dynamic mechanism of looseness, due to a corkscrew effect on the foundations [2]. If instead of the 2-pole induction motor, a 2-pole synchronous motor had been used, then the non-linear effect of rotor stiffness anisotropy would have further destabilized the system (Eq.23).

B. Business Case #2

Now knowing this mechanism, the end-user, the OEM, and the motor manufacturer decided to improve the design for the next project of LNG trains operating at similar speed range and power. The technical improvement points are as follows:

- keeping 2-pole induction rotor (Fig.18),
- increasing the system rigidity by decreasing the height of the skid, and increasing the height of concrete foundation (Fig.21),
- increasing the damping (D) of the bearings by changing 4-lobe bearings by tilting pads bearings,
- increasing natural frequency of reed mode.
- performing vibration tests in FAT on rigid soleplates and with the skid strongly fitted to the testbed foundation (Fig.19, 20 & 21).

Fig.18. 2-pole Induction Rotor.

Fig.19. Rigid soleplates.

Fig.20. Motor on rigid soleplates.

Fig.21. Rotor + Skid on rigid soleplates.

The stator is now fixed on a suspension to avoid a risk of reed mode excitation by the pole passing frequency of the motor at twice the electrical frequency of the drive (Fig.22). By adjusting the suspension frequency of the stator at low frequency (Fig.23), the transmission (T) of force from the stator (F_{stator}) to the frame (F_{stator}) is

greatly reduced thanks to the dynamic response of the suspension responding as a mass (Case #B):

$$T = \frac{F_{stator}}{F_{frame}} = \sqrt{\frac{1 + 4.\zeta_S^2}{\left(1 - f^2/f_{ss}^2\right)^2 + 4.\zeta_S^2}} \qquad (29)$$

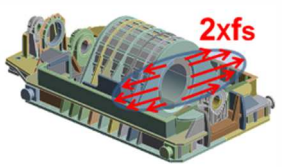

Fig.22. Example of 2-pole passing frequency excitation.

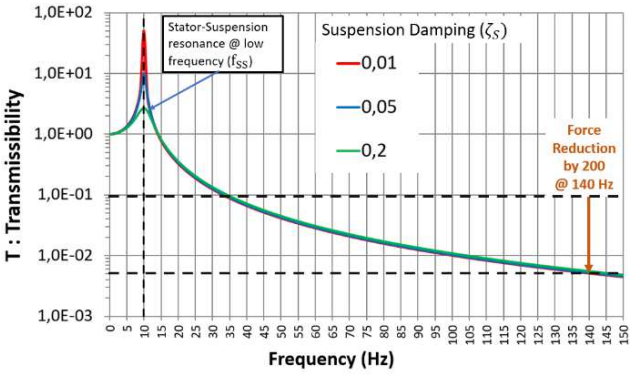

Fig.23. Stator-Suspension Transfer Function.

The vibration behavior of the motor bolted to the skid gives very good results, even in full load. The vibrations at the resonant frequencies of the rotor do not exceed 1.5 mm/s rms at the bearing locations (Fig.24) and 1 mm/s (Fig.25) at the motor feet with a good rigidity of the skid, without interaction with the reed mode.

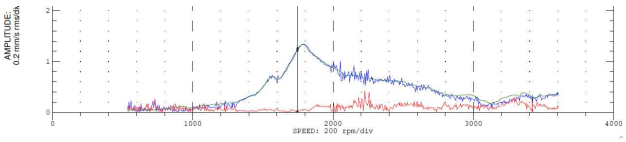

Fig.24. Motor Bearing Horizontal Vibration (Motor+Skid).

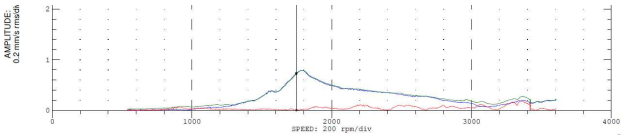

Fig.25. Motor Foot Horizontal Vibration (Motor+Skid).

The shaft displacements during full load test do not exceed 60 umpp at the location of the modes and 20 umpp in the contractual speed range (Fig.26).

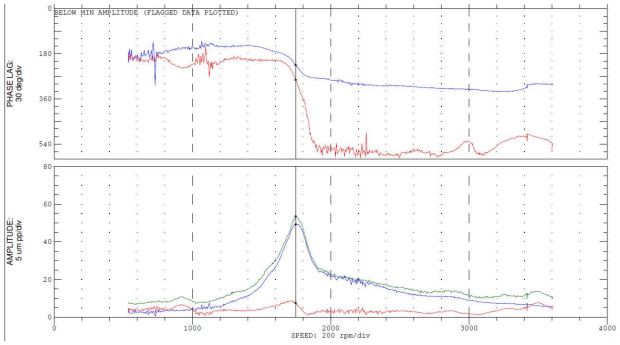

Fig.26. Shaft Displacement – Load Test (Motor+Skid).

C. Business Case #3

For an export compression service, the end-user has decided to replace for one of these offshore platforms in the North Sea, the existing turbines by 9kV 2-pole high-speed induction motors on active magnetic bearings 97.6%. efficiency, operating 16MW@8000rpm with a maximum continuous speed at 9000rpm (Fig. 28). This turbine replacement by electric drive has made it possible to reduce the weight of the embedded equipment and to avoid the platform sinking into the sea, increasing the flexibility of use at different speeds, and reducing the greenhouse gas emissions.

Fig. 27. Motor AMB.

Fig.28. 16MW@8000 rpm 2-pole induction motor on AMB(s).

The electromagnet pulling force of the AMB(s) is given as follow (Fig.27):

$$F_{pull} = (\sigma_{mag}).A = \left(B_{airgap}^2 \Big/ 8\pi\ 10^{-7}\right).A \qquad (30)$$

The magnetic induction in the airgap (B_{airgap}) is of the order of 1.5 Tesla because of magnetic saturation in the laminations of the bearing, generating a magnetic pressure around 1 N/mm² and magnetic stiffness around 10^{-3} N/m. The stiffness of AMB is very soft compared to an oil film. The magnetic bearings avoid any modes in the operating speed range of the system. The rotor is operating in subcritical free-free mode when using magnetic bearings, meaning that the first bending mode is above operating speed (Fig.29):

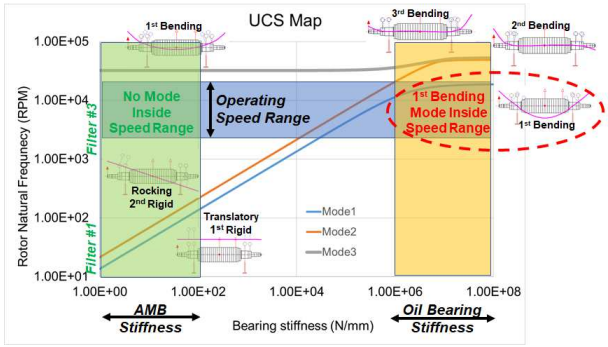

Fig.29. Example of undamped critical speed map of a 7MW@13,000rpm export compressor motor [9].

Vibrations at full load at 9000rpm are less than 50umpp (Fig.30) with an alarm and trigger threshold set by mutual agreement with the end user at 100umpp and 150umpp. The stiffness of AMB is frequency controlled, with zero stiffness injection at the rotational frequency, the rotor spinning around its instantaneous center of inertia (Fig.31). This makes it possible to inject no unbalance force into the structures of the platform, avoiding possible resonances compared to an arrangement on oil bearings even with flexible offshore structure.

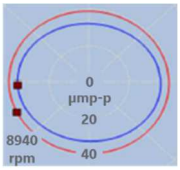

Fig.30. Shaft orbits @ 8940rpm.

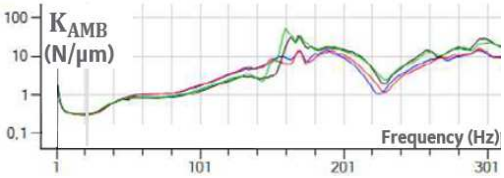

Fig.31. AMB stiffness vs Frequency.

More globally, this high-speed direct drive system architecture using 2-pole induction motor on AMB(s) brings substantial reduction in weight and footprint reducing the size of the topside structure and its associated cost for a green field project. A typical cost ratio of 10 to 20 k$ per ton of installed base is the usual assumption for offshore structure.

IV. CONCLUSIONS AND RECOMMANDATIONS

This publication makes it possible to understand certain non-linear vibration mechanisms related to rotating machines, especially for variable high-speed 2-pole electric motors. The return of experience of three business cases from the end-user and the motor manufacturer makes it possible to formulate recommendations that are sometimes more restrictive than the acceptance criteria of API 541 and 546. It is recommended to share and discuss the following design rules and tests procedures between the End-user, the EPC, the OEM, and the Electrical System Manufacturer during the tendering phase of the project:

- No natural frequency of rotor bending in the 1X or 2X variable speed range,
- No natural frequency of the end-shields of the frame in the 1X and 2X variable speed range,
- No global “reed” mode of structure bending (horizontal or axial) in the ½X, 1X and 2X variable speed range, or close to the rotor bending natural frequencies avoiding any risk of modal chaotic couplings and rotor instability,
- Skid vibration near the motor feet to be less than 60% of the vibration measured at the bearings,
- Increasing the system rigidity by decreasing the height of the skid, and increasing the height of concrete foundation,
- Increasing the damping of the bearings by changing 4-lobe bearings to tilting pads bearings,
- Using AMB(s) on flexible foundation as for offshore structure,
- Using a stator suspension to avoid reed mode excitation,
- Performing vibration tests in FAT on rigid soleplates and with the skid strongly fitted to the testbed foundation,
- Checking 2-pole synchronous rotor cross-section anisotropy,
- Rotor overspeed at rated speed +20% with three cold-hot cycles of temperatures for unbalance stability check.
- Full load test or alternative heating tests for assessing rotor thermal stability with three consecutive cold-hot cycles of temperatures, and the stator temperature rise,
- Performing string tests with the full equipped moto-compressor on its skid, the compressor unit control panel, the cables, the VSDS in its shelter, the transformer, and the turbine in case of helper motor configuration,
- Vibrations checks at all loads and speeds during site commissioning.

By following all these recommendations, it will be possible to avoid problems during commissioning of compressor trains or turbine replacements, reducing project execution lead time, and at the end taking advantage of all the operational flexibility of variable speed electrical systems including the reduction of greenhouse gases emissions.

V. ACKNOWLEDGEMENTS

Thanks to Olivier Gorieu (Senior Project Engineer at TotalEnergies TGI) for supporting this paper, Alexandre Kral (SKF-S2M) for contributing to this paper, and Alfred Permuy (GE PC) for educating the team on the parametric properties of the Hill-Mathieu’s differential equations.

VI. REFERENCES

[1]. L. Durantay, T. Clark, J. Paschal, N. Spolvery, L. Roth, P.P. Vivier, “Innovative Solution for Large LNG Compression Trains Using 2-pole Induction Helper Motor fed by VSI”, in Proc. 48th TPS, Houston, 2019.

[2]. C. Scheffer, P. Girdhar, “Machinery Vibration Analysis & Predictive Maintenance”, Newnes-Elsevier Ed., 2004.

[3]. R. Campbell, “Théorie Générale de l’Equation de Mathieu et de quelques autres équations différentielles de la Mécanique”, Masson Ed., 1955.

[4]. C.W. Lee, “Vibration Analysis of Rotors”, Kluber Academic Publishers Ed., 1993.

[5]. A. Muszynska, “Rotordynamics”, Taylor & Francis Ed., 2005.

[6]. T. Krysinski, F. Malburet, “Instabilité mécanique, contrôles actifs et passifs”, Lavoisier Editions, 2009.

[7]. L. Durantay, D. Van Gemert, J. Lava, D. Spannagel, “A Success Story of Steam Turbine Replacement by High-Speed Electric System Driven Compressor”, in Proc. IEEE-PCIC Europe Conference, 2021.

[8]. W.R. Finley, R.R. Burke, “Troubleshooting Motor Problems”, IAS, 1993, IEEE Transactions of Industry Applications, 1994, vol.30, no. 5.

[9]. L. Durantay, Th. Alban, S. Siala, A. Billaud, “Selections and Tests of Innovative Variable Speed Motor-Compressor Solutions for a 55MW Full Electric Offshore Platform Maximizing Availability and Efficiency with Better Environmental Impact”, in Proc. IEEE-PCIC Conference, Cincinnati, 2018.

VII. NOMENCLATURE

M	System Mass M (kg).	U	Displacement (m).
D	System Damping (N.s/m).	$\dot{U}$	Speed (m/s).
K	System Stiffness (N/m).	$\ddot{U}$	Acceleration (m/s²).
t	Time (s).	$f(t)$	Time Function.
n	Integer Indices.	ω_0	Critical Pulsation (rad/s).
ζ	System Damping Coefficient.	a_n	Fourier coefficient.
Ω	Speed (rad/s).	Φ_n	Fourier phase (rad).
$\langle I_n \rangle$	Instable bandwidth (rad/s).	$\bar{\lambda}$	Complex Eigen Value.
Δ_n	Complex Pulsation Range (rad/s).	D_I	Rotor Damping (N.s/m)
φ	Phase (rad/s).	(ξ, η)	Rotor Axis System.
K_ξ, K_η	Rotor Asymmetric Stiffness (N/m).	F_M	Inertial Force (N).
M_ξ, M_η	Rotor Asymmetric Mass (Kg).	F_K	Spring Force (N).
D_ξ, D_η	Rotor Asymmetric Damping (N.s/m).	F_D	Damping Force (N).
ω_ξ, ω_η	Rotor Asymmetric Critical Pulsation (Rad/s).	F_{D_I}	Instability Force (N).
D_B	Bearing Damping (N.s/m).	K_B	Bearing Stiffness (N/m).
j	Complex Number.	(X,Y,Z)	Fixed Cartesian Axis.
ζ_S	Suspension Damping Coefficient.	F_{stator}	Stator Force (N).
ω_{a0}	Average Circular Pulsation (Rad/s).	μ	Asymmetry Coefficient.
f_{ss}	Stator-Suspension Critical Frequency (Hz).	F_{frame}	Frame Force (N).
f	Frequency (Hz).	T	Transmissibility Coefficient.
Ω_{op}	Operating Pulsation (Rad/s).	$\langle \Omega_{op} \rangle$	Speed Range (Rad/s).
Ω_{el}	Electrical Pulsation (Rad/s).	$\langle \Omega_{el} \rangle$	Electrical Range (Rad/s).
B_{airgap}	Airgap Induction (T).	A	AMB Airgap Surface (m²).
σ_{mag}	Magnetic Pressure (N/m²).	F_{pull}	AMB Pulling Force (N).

AMB	Active Magnetic Bearing.
CDS	Complex Dynamic Stiffness.
DFE	Diodes Front End.
FFT	Fast Fourier Transformation.
LCI	Load Commutated Inverter.
LNG	Liquefied Natural Gas.
VSD	Variable Speed Drive.
VSI	Voltage Source Inverter.

VIII. VITA

Lionel DURANTAY is graduated from the Ecole Nationale Supérieure d’Electricité et de Mécanique (ENSEM) in Nancy, France with an engineering degree in 1989 then passed PhD in 1993. As R&D Leader, he has developed innovative variable speed motors & generators solutions for Oil & Gas, offshore renewable and marine businesses. He has authored or coauthored 50+ technical papers. He presently holds 20+ patents. He is currently Global Product & Technology Leader within GE Power Conversion.

Alain GELIN graduated from the INSA Lyon (Institut National des Sciences Appliquées) with a mechanical engineering degree in 1987 then passed PhD in 1990. He is worked 20 years for GE Oil&Gas as R&D Mechanical Engineer and Testing Dept Manager. Joining TOTAL in 2005, he is involved in the development schemes for compression and in qualification programs. He has authored 20+ technical papers in dynamics. He is currently Senior Rotating Equipment at TotalEnergies E&P Head.

Edouard THIBAUT is graduated as an electrical engineer from the Ecole Supérieure d’Ingénieurs en Electronique et Electrotechnique (ESIEE). Before joining TotalEnergies in 2009, he worked eleven years for Alstom Power Conversion and then Converteam. He held several positions as Variable Speed Drive Systems design and commissioning engineer in several major international projects both Onshore and Offshore in Europe, Asia, and North America. He has authored or coauthored 24 technical papers. He presently holds 3 patents. He is currently Electrical Specialist for various projects within TotalEnergies.

Lionel ROTH is graduated from the ENIM (Ecole Nationale des Ingénieurs de Metz) in Mechanical Engineering, in 2006. He led several induction and synchronous motors customization fed by VSDS for Oil & Gas Business. He has coauthored 3 technical papers. He is currently Lead Technical Project Manager in GE’s rotating machines group.